3-17-2020

Chromatin-binding protein PHF6 regulates activity-dependent transcriptional networks to promote hunger response

Linhua Gan
Shanghai Jiaotong University
Cheng Cheng
Washington University School of Medicine in St. Louis
Azad Bonni
Washington University School of Medicine in St. Louis
et al

Article

Cell Reports

Chromatin-Binding Protein PHF6 Regulates Activity-Dependent Transcriptional Networks to Promote Hunger Response

Graphical Abstract

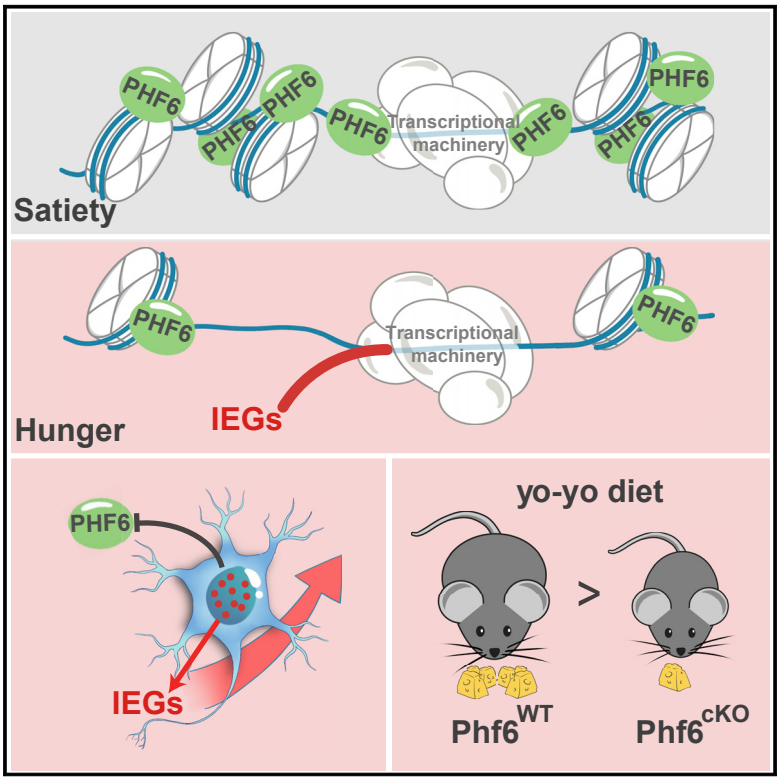

Highlights

- PHF6 is a transcriptional repressor regulating IEG expression in AgRP neurons
- PHF6-chromatin binding is dynamically regulated by different nutritional states
- Loss of PHF6 in AgRP neurons impairs hunger-induced gene transcription
- Loss of PHF6 in AgRP neurons decreases hunger-driven feeding motivation

Authors

Linhua Gan, Jingjing Sun, Shuo Yang, ..., Azad Bonni, Qian Li, Ju Huang

Correspondence

liqian@shsmu.edu.cn (Q.L.), juhuang@shsmu.edu.cn (J.H.)

In Brief

Gan et al. show that PHF6 is a transcriptional repressor enriched in AgRP neurons and regulates immediate-early gene (IEG) expression. Depletion of PHF6 in AgRP neurons decreases hunger-driven feeding motivation and makes the mice resistant to body weight gain under repetitive fasting/refeeding conditions.

Gan et al., 2020, Cell Reports *30*, 3717–3728
March 17, 2020
https://doi.org/10.1016/j.celrep.2020.02.085

CellPress

Cell Reports
Article

Chromatin-Binding Protein PHF6 Regulates Activity-Dependent Transcriptional Networks to Promote Hunger Response

Linhua Gan,[1,12] Jingjing Sun,[1,12] Shuo Yang,[1] Xiaocui Zhang,[2] Wu Chen,[6] Yiyu Sun,[3] Xiaohua Wu,[1] Cheng Cheng,[5] Jing Yuan,[6,7] Anan Li,[6,7] Mark A. Corbett,[8] Mathew P. Dixon,[9] Tim Thomas,[9,10] Anne K. Voss,[9,10] Jozef Gécz,[8] Guang-Zhong Wang,[11] Azad Bonni,[5] Qian Li,[1,4,*] and Ju Huang[1,4,13,*]

[1]Collaborative Innovation Center for Brain Science, Department of Anatomy and Physiology, Shanghai Jiao Tong University School of Medicine, Shanghai 200025, China
[2]Core Facility of Basic Medical Sciences, Basic Medicine Faculty of Shanghai Jiao Tong University School of Medicine, Shanghai 200025, China
[3]Department of Neurosurgery, Shanghai Ninth People's Hospital, Shanghai Jiao Tong University School of Medicine, Shanghai 201999, China
[4]Shanghai Research Center for Brain Science and Brain-Inspired Intelligence, Shanghai 201210, China
[5]Department of Neuroscience, Washington University School of Medicine, St. Louis, MO 63110, USA
[6]Britton Chance Center for Biomedical Photonics, Wuhan National Laboratory for Optoelectronics-Huazhong University of Science and Technology, Wuhan, Hubei 430074, China
[7]HUST-Suzhou Institute for Brainmatics, Suzhou 215125, China
[8]Adelaide Medical School, The University of Adelaide, Adelaide, SA, Australia
[9]The Walter and Eliza Hall Institute of Medical Research, Melbourne, VIC, Australia
[10]Department of Medical Biology, The University of Melbourne, VIC, Australia
[11]CAS Key Laboratory of Computational Biology, CAS-MPG Partner Institute for Computational Biology, Shanghai Institute of Nutrition and Health, Chinese Academy of Sciences, Shanghai 200031, China
[12]These authors contributed equally
[13]Lead Contact
*Correspondence: liqian@shsmu.edu.cn (Q.L.), juhuang@shsmu.edu.cn (J.H.)
https://doi.org/10.1016/j.celrep.2020.02.085

SUMMARY

Understanding the mechanisms of activity-dependent gene transcription underlying adaptive behaviors is challenging at neuronal-subtype resolution. Using cell-type specific molecular analysis in agouti-related peptide (AgRP) neurons, we reveal that the profound hunger-induced transcriptional changes greatly depend on plant homeodomain finger protein 6 (PHF6), a transcriptional repressor enriched in AgRP neurons. Loss of PHF6 in the satiated mice results in a hunger-state-shifting transcriptional profile, while hunger fails to further induce a rapid and robust activity-dependent gene transcription in PHF6-deficient AgRP neurons. We reveal that PHF6 binds to the promoters of a subset of immediate-early genes (IEGs) and that this chromatin binding is dynamically regulated by hunger state. Depletion of PHF6 decreases hunger-driven feeding motivation and makes the mice resistant to body weight gain under repetitive fasting-refeeding conditions. Our work identifies a neuronal subtype-specific transcriptional repressor that modulates transcriptional profiles in different nutritional states and enables adaptive eating behavior.

INTRODUCTION

Hunger-driven feeding behavior is regulated by agouti-related peptide (AgRP) neurons in the arcuate nucleus (ARC) of the hypothalamus. AgRP neurons play a critical role in linking the energy-deficient sensation with the decision to seek and consume food (Atasoy et al., 2012; Gropp et al., 2005; Sternson and Eiselt, 2017; van den Top et al., 2004). Activation of AgRP neurons rapidly increases food intake (Aponte et al., 2011; Krashes et al., 2011), while ablation of AgRP neurons in adulthood results in starvation (Luquet et al., 2005). Hunger induces dramatic changes in transcription profiles of AgRP neurons (Henry et al., 2015). However, the upstream transcriptional factors or epigenetic regulators (histone acetyltransferases, methyltransferases, chromatin-remodeling enzymes, etc.) that affect the downstream hunger-responsive gene expression in AgRP neurons under different nutritional states are still unknown.

In the nervous system, activity-dependent gene transcription facilitates the execution of innate, homeostatic, and learned behaviors. Despite substantial progress in the field of activity-dependent gene transcription, how this process influences behavioral adaptation and instructs changes to dynamic behavioral states is not completely known. Its regulation is dependent on the concerted execution of upstream transcriptional and epigenetic regulators. Recent advances suggest that many activators are recruited to the promoters of the immediate-early genes (IEGs) to facilitate their transcription, while repressors, including the inhibitory transcription factors and architectural

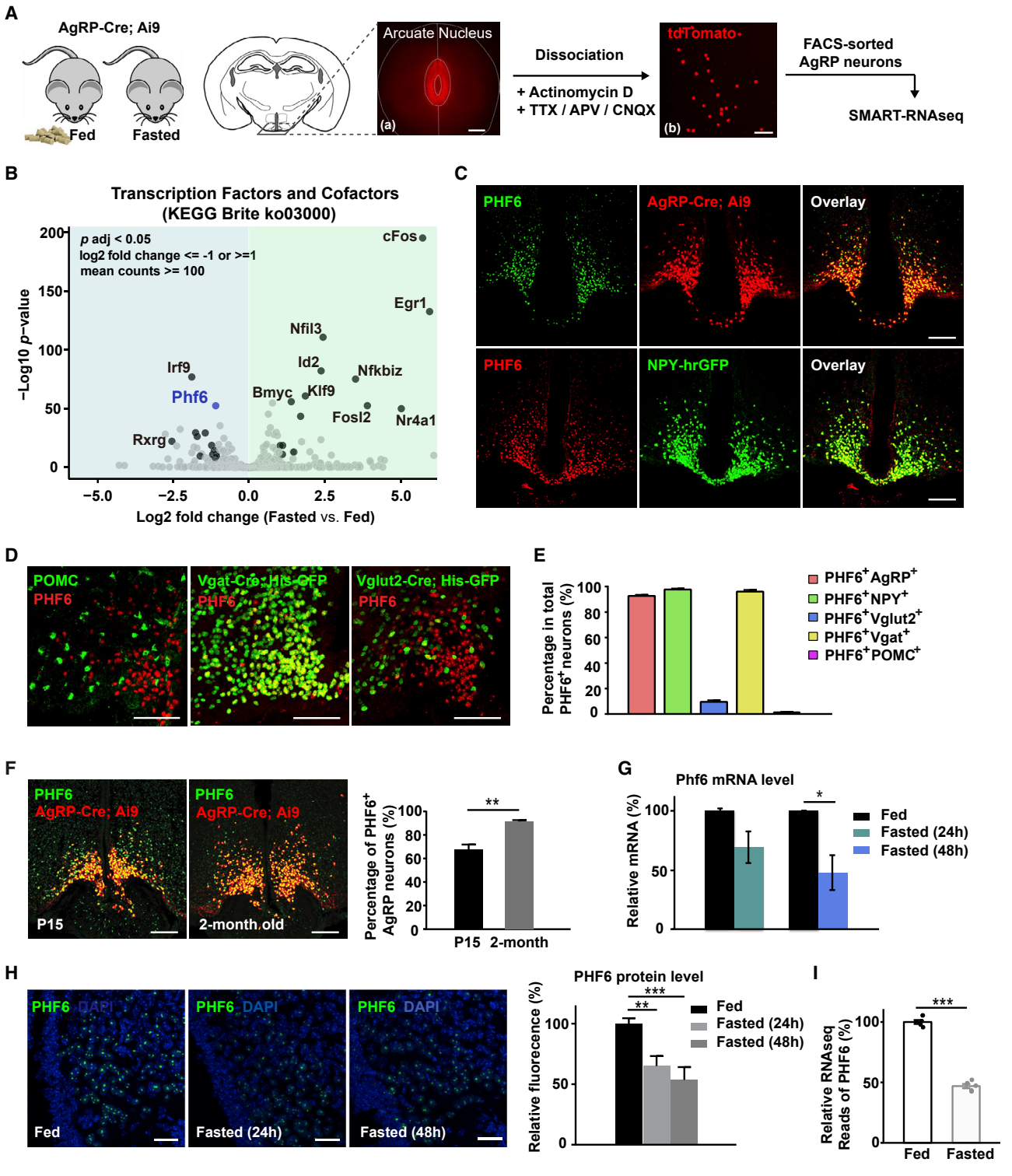

Figure 1. PHF6 Is Enriched in AgRP Neurons and Downregulated in Hunger

(A) Illustration of SMART-RNA-seq analysis from FACS-sorted tdTomato$^+$ AgRP neurons from AgRP-Cre; Ai9 mice under fed and fasting conditions. Scale bars are 0.4 mm (a) and 100 μm (b).

(B) RNA-seq analysis was performed on the transcription factor and cofactors based on the list of KEGG Brite ko03000 under fasting conditions (n = 5) and fed conditions (n = 5) in WT mice.

(legend continued on next page)

constraining proteins, suppress IEG expression under basal conditions (Kim et al., 2010; Madabhushi et al., 2015; Madabhushi and Kim, 2018; Yap and Greenberg, 2018).

In the context of hunger-driven feeding behavior, we hypothesize that hunger state drives the release or downregulation of such transcriptional repressors to facilitate the hunger-driven gene expression. In the present study, we investigate the transcriptional profiles of AgRP neurons in different nutritional states. We identify plant homeodomain finger protein 6 (PHF6) as an AgRP-neuron-enriched transcriptional repressor that regulates the expression of activity-dependent IEGs. We further investigate the molecular mechanisms by PHF6 chromatin immunoprecipitation sequencing (ChIP-seq) analysis on enriched ARC tissues. Our results provide a perspective on how transcriptional modulation in defined neurons shapes the behavioral output of the animal.

RESULTS

PHF6 Is Highly Enriched in AgRP Neurons and Downregulated in Hunger

We performed SMART-RNA sequencing (RNA-seq using Smart-seq2 method) analysis on florescence-activated cell sorting (FACS)-sorted tdTomato-positive AgRP neurons from 3- to 4-week-old AgRP-Cre; Ai9 mice under fed and fasted conditions (Figure 1A). We used a method to enable the faithful detection of both baseline and physiologically induced transcriptional features by applying a cocktail of inhibitors that block transcription, neuronal activity, and calcium entry (Hrvatin et al., 2018; Wu et al., 2017). We first validated the quality of our SMART-RNA-seq data by showing the positive correlation of the fold changes of gene expression under fasted versus fed conditions between our experiment and the sequencing data from a previous study (Figure S1A).

Next, we analyzed the changes in transcription factors and cofactors based on the list of Kyoto Encyclopedia of Genes and Genomes (KEGG) Brite: ko03000. We found that a subset of transcription factors and cofactors were significantly upregulated or downregulated in AgRP neurons in the hunger state (Figure 1B; Table S1). Despite the equal importance of the upregulated genes and downregulated genes, here we focused on the downregulated ones. We speculated that those downregulated genes might include transcriptional repressors suppressing hunger-dependent gene transcription under basal conditions. Among them, we found that the Börjeson-Forssman-Lehmann syndrome (BFLS) protein, PHF6, showed highly enriched expression in the ARC of the hypothalamus (Figures 1B and 1C).

PHF6 expresses and functions in the early brain development (Cheng et al., 2018; Voss et al., 2007; Zhang et al., 2013). However, the role of PHF6 in the adult brain is not well characterized. Here, we examined the expression of PHF6 in the adult mice brain using a specific anti-PHF6 antibody, and the specificity of the antibody was validated using PHF6-deficient ($Phf6^{C99F}$) mice (Cheng et al., 2018; Figure S1B). PHF6 was enriched in four subcortical areas in the adult brain, including the ARC, the median preoptic area (mPOA), the ventral pallidum (VP), and the supraoptic nucleus (SON) (Figure S1C). In contrast, PHF6 expression was almost diminished in the cortex and hippocampus in the adult brain (Figure S1E). Using Vgat-Cre and Vglut2-Cre reporter mice, we found that most of the PHF6-positive neurons in the ARC, mPOA, and VP were GABAergic, while most of the PHF6-positive neurons in the SON were glutamatergic (Figures S1D and 1D).

Using AgRP-Cre; Ai9 and neuropeptide Y (NPY)-hrGFP mice having tdTomato and hrGFP in the hypothalamic AgRP/NPY neurons, we found that more than 90% of the PHF6-positive neurons in the ARC colocalized with the AgRP-positive and NPY-positive neurons (Figures 1C and 1E). None of the PHF6-positive neurons colocalized with the hypothalamic proopiomelanocortin (POMC) neurons (Figures 1D and 1E). We observed a higher percentage of PHF6-positive AgRP neurons in 2-month-old mice (91% ± 1%) than in postnatal day 15 (P15) mice (68% ± 4%) (Figure 1F). These results indicate that PHF6 is highly enriched in hypothalamic AgRP neurons in the adult mice.

We then determined the dynamic changes in PHF6 expression in different nutritional states of the mice. Under the conditions of 24-h and 48-h hunger stimulations, we found that both the mRNA and protein levels of PHF6 in the ARC were reduced by approximately 40% and 60%, respectively (Figures 1G and 1H). Further analysis of PHF6 protein levels in a single AgRP neuron showed that 33.6% ± 11.5% and 61.6% ± 14.6% of AgRP neurons showed a more than 50% reduction under 24-h and 48-h fasted conditions, respectively (Figures S2A and S2B). SMART-RNA-seq from FACS-sorted AgRP neurons in the wild-type (WT) mice also confirmed a reduction magnitude of approximately 50% in the Phf6 mRNA level

(C) Immunofluorescence of endogenous PHF6 in the ARC of AgRP-Cre; Ai9 mice in which AgRP/NPY neurons were labeled with tdTomato, and NPY-hrGFP mice in which AgRP/NPY neurons were labeled with hrGFP. The scale bars are 100 μm.
(D) Immunofluorescence of endogenous PHF6 and POMC in the ARC of WT mice. Immunofluorescence of endogenous PHF6 in the ARC of Vgat-Cre, histone-GFP and Vglut2-Cre, and histone-GFP mice, in which the GABAergic and glutamatergic neurons were labeled with nuclear histone-conjugated GFP. The scale bars are 75 μm.
(E) Quantification of the percentage of $PHF6^+AgRP^+$, $PHF6^+NPY^+$, $PHF6^+Vglut2^+$, $PHF6^+Vgat^+$, and $PHF6^+POMC^+$ neurons in total $PHF6^+$ neurons in the ARC (n = 3 for each).
(F) Immunofluorescence of PHF6 and quantification of the percentage of $PHF6^+AgRP^+$ neurons in total $PHF6^+$ neurons in the ARC of P15 (n = 3) and 2-month-old (n = 3) AgRP-Cre; Ai9 mice ($p < 0.01$). The scale bars are 100 μm.
(G) Quantification of the relative mRNA level of PHF6 by quantitative PCR under fed conditions, 24-h fasting conditions (n = 3), and 48-h fasting conditions (n = 4, $p < 0.05$).
(H) Immunofluorescence of PHF6 and quantification of relative PHF6 fluorescent signal in the ARC of 7-week-old WT mice under fed conditions (n = 7), 24-h fasting conditions (n = 6, $p < 0.01$), and 48-h fasting conditions (n = 6, $p < 0.001$). The scale bars are 25 μm.
(I) Quantification of normalized counts of PHF6 from the SMART-RNA-seq dataset under fed conditions (n = 5) and fasting conditions (n = 5, $p < 0.001$).
Data are represented as mean ± SEM. See also Figure S1 and Table S1.

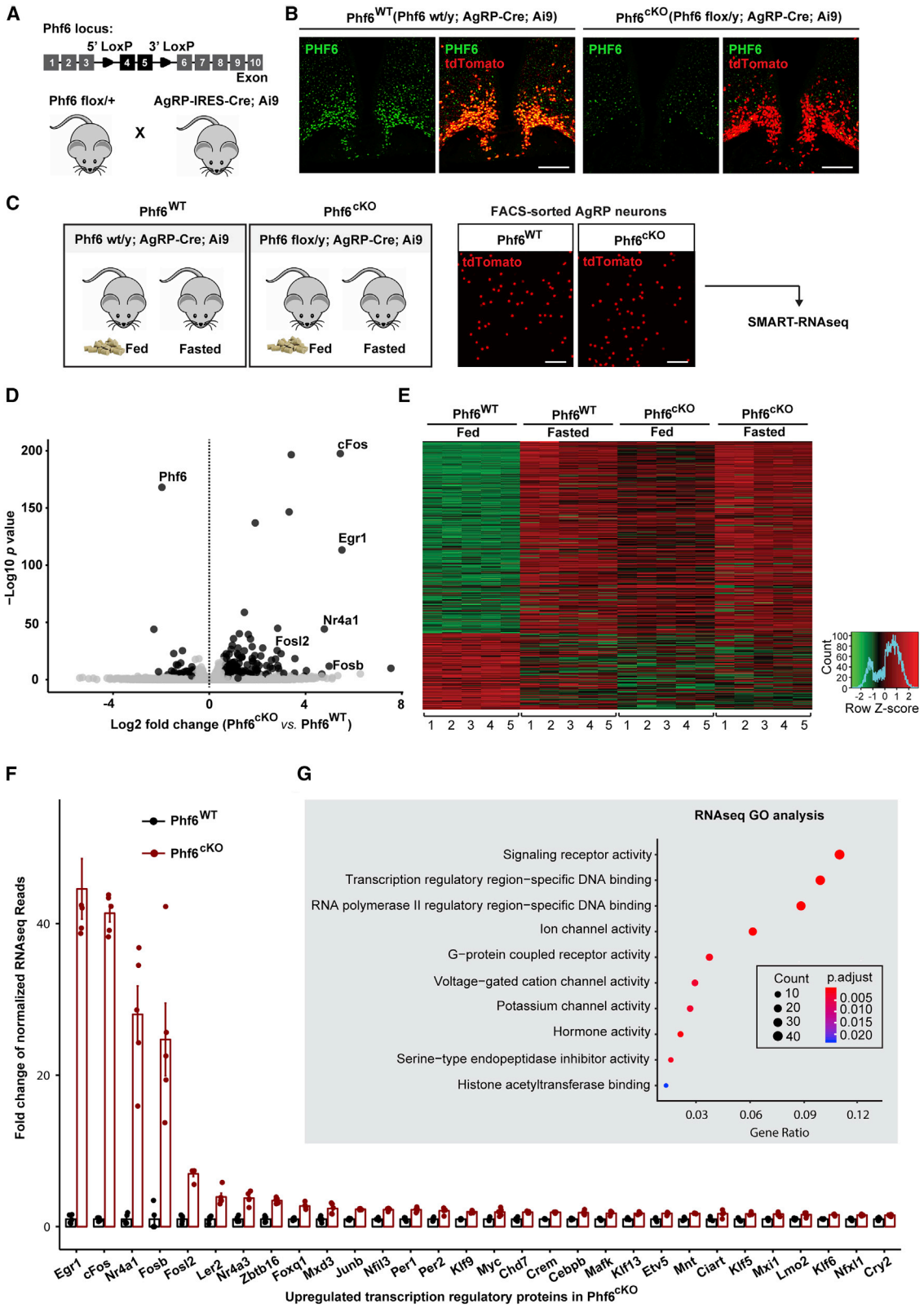

(legend on next page)

under the condition of overnight fasting (Figure 1I). These findings indicate that PHF6 is downregulated in AgRP neurons in the hunger state.

PHF6 Suppresses IEG Expression in AgRP Neurons

Given the enriched expression of PHF6 in AgRP neurons and its downregulation in hunger, we investigated whether PHF6 is critically involved in hunger-dependent transcriptional regulation. We generated conditional Phf6 knockout mice in AgRP neurons by crossing mice harboring a floxed allele of the Phf6 gene that contains loxP sites flanking its exons 4 and 5 in the X chromosome (McRae et al., 2019) with AgRP-Cre; Ai9 mice (Figure 2A). Disruption of the Phf6 gene in Phf6 conditional knockout mice (referred to as $Phf6^{cKO}$) resulted in a marked loss of the PHF6 protein in AgRP neurons (Figure 2B). We performed SMART-RNA-seq in FACS-sorted tdTomato-positive AgRP neurons from both $Phf6^{cKO}$ and $Phf6^{WT}$ mice under fed and fasted conditions (Figure 2C). To enable the faithful detection of the transcriptomes, a cocktail of inhibitors that block transcription, neuronal activity, and calcium entry was applied. Pairwise differential expression analysis of the transcriptomes from AgRP neurons in $Phf6^{WT}$ and $Phf6^{cKO}$ mice indicated that a loss of PHF6 caused marked changes in the transcription profile of AgRP neurons. Apart from a significantly reduced Phf6 mRNA level, we identified 421 differentially expressed genes in $Phf6^{cKO}$ AgRP neurons compared to those in $Phf6^{WT}$ AgRP neurons, passing the threshold of false discovery rate (FDR) adjusted p value (p adj) <0.05, fold change >1.5 (upregulated) or fold change <0.67 (downregulated), mean of normalized counts ≥ 20 (Figures 2D and 2E; Table S2). We observed substantially more upregulated genes than downregulated genes in the $Phf6^{cKO}$ AgRP neurons (Figures 2D and 2E), indicating that PHF6 mainly functions as a transcriptional repressor or as part of a repressive complex rather than as a transcriptional activator in AgRP neurons.

Gene Ontology (GO) analysis showed that the differentially expressed genes between the $Phf6^{WT}$ and $Phf6^{cKO}$ AgRP neurons were significantly enriched in functional classes including signaling receptors, transcription regulatory region-specific DNA-binding proteins, and ion channels (Figure 2G). PHF6 regulated the expression of many transcription regulatory proteins, indicating that PHF6 might be the upstream regulator of other transcription factors in AgRP neurons. Strikingly, we found that the basal levels of many neuronal-activity-dependent IEGs—including Egr1, cFos (Fos), Nr4a1, Fosb, and Fosl2—were dramatically upregulated in $Phf6^{cKO}$ AgRP neurons compared to those in $Phf6^{WT}$ AgRP neurons under basal conditions (Figure 2F). Notably, we observed that a loss of PHF6 in AgRP neurons led to a comparatively larger magnitude of changes in the mRNA levels of activity-dependent IEGs than other transcription factors. Loss of PHF6 in AgRP neurons caused more than 40-fold increases in the expression of Egr1 and cFos, as well as more than 20-fold increases in the expression of Nr4a1 and Fosb (Figure 2F). Therefore, these results suggest that PHF6 functions as a critical upstream transcriptional repressor to suppress the expression of a subset of IEGs and that a loss of PHF6 leads to sustained increases of these IEGs in AgRP neurons in the satiety state.

The quadrant-wise analysis of differentially expressed genes in SMART-RNA-seq data ($Phf6^{WT}$-fed; $Phf6^{cKO}$-fed; $Phf6^{WT}$-fasted; $Phf6^{cKO}$-fasted) revealed that the majority of genes upregulated in $Phf6^{cKO}$ mice compared to those in $Phf6^{WT}$ mice were also increased in WT AgRP neurons in the hunger state (Figure 2E). We next performed a gene set enrichment analysis (GSEA), and this analysis also revealed that the genes upregulated upon a PHF6 loss were significantly enriched in the hunger-responsive upregulated gene set in WT mice (Figure 3A). These results suggest that a loss of PHF6 causes a hunger-state shifting transcriptional profile of AgRP neurons even in satiated mice. Although PHF6 loss made the AgRP neurons look transcriptionally more similar to AgRP neurons in the hunger state, there were still approximately 13% of the $Phf6^{cKO}$-related differentially expressed genes that showed opposite trends between changes in $Phf6^{cKO}$-fed versus $Phf6^{WT}$-fed and changes in $Phf6^{WT}$-fasted versus $Phf6^{WT}$-fed (Figure S3A), suggesting that the changes in transcription profiles caused by Phf6 knockout and by hunger stimulation are not equal.

Hunger State Fails to Further Induce a Rapid Induction of IEGs in Phf6-Deficient AgRP Neurons

While many activity-dependent IEGs were constitutively increased in the $Phf6^{cKO}$ AgRP neurons in basal conditions, the hunger-induced fold changes of these IEGs were markedly reduced in $Phf6^{cKO}$ mice compared to those in $Phf6^{WT}$ mice (Figure 3B; Table S3). Certain IEGs were even repressed in $Phf6^{cKO}$ mice in fasted conditions. For examples, hunger-induced fold

Figure 2. PHF6 Suppresses Basal IEG Expression in AgRP Neurons in the Satiety State

(A) Strategy to generate the conditional Phf6 knockout mice.

(B) Immunofluorescence of endogenous PHF6 in the ARC from $Phf6^{WT}$ and $Phf6^{cKO}$ mice in which AgRP neurons expressed tdTomato. The scale bars are 100 μm.

(C) Illustration of SMART-RNA-seq analysis from FACS-sorted $tdTomato^{+}$ AgRP neurons in $Phf6^{WT}$ and $Phf6^{cKO}$ mice under fed and fasting conditions. The scale bars are 100 μm.

(D) Log2-fold change in the normalized counts of RNA-seq reads of differentially expressed genes in AgRP neurons from $Phf6^{cKO}$ mice ($n = 5$) and $Phf6^{WT}$ mice ($n = 5$).

(E) Heatmap of the quadrant-wise analysis of differentially expressed genes in $Phf6^{WT}$ and $Phf6^{cKO}$ mice under both fed and fasting conditions. The heatmap illustrated 421 differentially expressed genes in $Phf6^{cKO}$ AgRP neurons (as compared to $Phf6^{WT}$ AgRP neurons in fed condition), cutoffs at FDR p adj <0.05, fold change >1.5 or <0.67, mean of normalized counts ≥ 20.

(F) Fold change in the normalized counts of RNA-seq reads for the upregulated genes in $Phf6^{cKO}$ AgRP neurons within the molecular pathway of a transcriptional regulatory protein.

(G) GO analysis for functional classes in which differentially expressed genes in $Phf6^{cKO}$ mice were enriched.

Data are represented as mean ± SEM. See also Figure S2 and Tables S2 and S3.

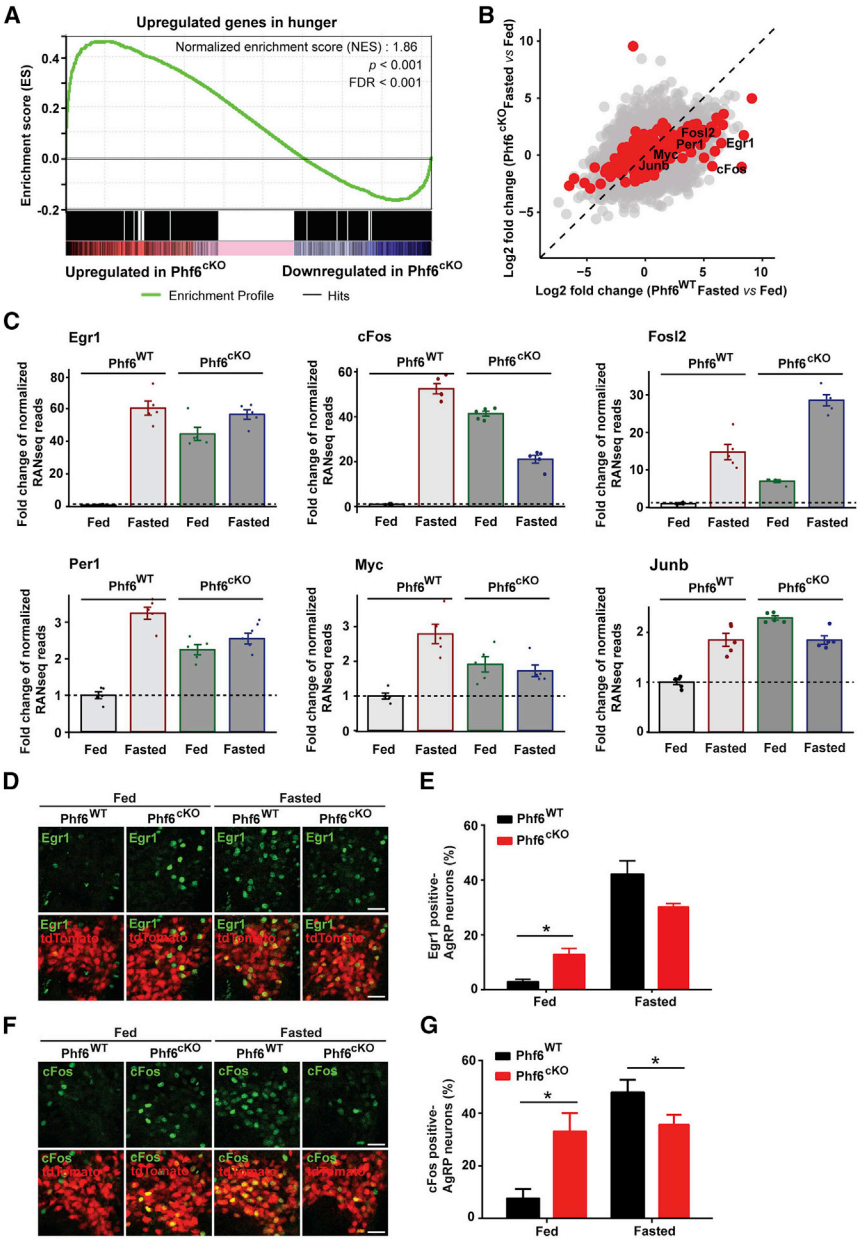

Figure 3. Decreased Hunger-Triggered IEG Induction in Phf6^{cKO} AgRP Neurons

(A) GSEA revealed that the upregulated genes in Phf6^{cKO} mice were enriched for hunger-responsive upregulated genes in WT mice (Normalized Enrichment Score [NES] = 1.86, p < 0.001, FDR < 0.001).

(B) Log2-fold changes in genes under fasting versus fed conditions in both Phf6^{cKO} mice and Phf6^{WT} mice were plotted (n = 5 for Phf6^{WT}-fed, n = 5 for Phf6^{WT}-fasted, n = 5 for Phf6^{cKO}-fed, and n = 5 for Phf6^{cKO}-fasted).

(C) Fold changes in normalized counts of RNA-seq reads of cFos, Egr1, Fosl2, Per1, Myc, and Junb under fasting versus fed conditions in Phf6^{WT} mice (n = 5) and Phf6^{cKO} mice (n = 5).

(D and F) Immunostaining of endogenous Egr1 (D) and cFos (F) under fed and fasting conditions in Phf6^{WT} and Phf6^{cKO} mice in which AgRP neurons were labeled with tdTomato. The scale bars are 25 μm.

(E) Quantification of the percentage of Egr1-positive AgRP neurons under fed and fasting conditions (n = 3 for Phf6^{WT}-fed, n = 3 for Phf6^{cKO}-fed, n = 3 for Phf6^{WT}-fasted, and n = 3 for Phf6^{cKO}-fasted).

(G) Quantification of the percentage of cFos-positive AgRP neurons under fed and fasting conditions (n = 3 for Phf6^{WT}-fed, n = 3 for Phf6^{cKO}-fed, n = 5 for Phf6^{WT}-fasted, and n = 5 for Phf6^{cKO}-fasted).

Data are represented as mean ± SEM. See also Figure S3 and Table S3.

changes in Egr1, Fosl2, and Per1 were reduced in Phf6^{cKO} mice, whereas hunger-induced fold changes in cFos, Myc, and Junb were repressed in Phf6^{cKO} mice (Figure 3C; Table S3).

We further validated this finding by immunohistochemistry using anti-Egr1 and anti-cFos antibodies. Under fed conditions, Phf6^{cKO} mice had significantly more Egr1-positive AgRP neurons (Figures 3D and 3E) and cFos-positive AgRP neurons (Figures 3F and 3G) in the ARC compared to Phf6^{WT} mice. In addition, we used the Phf6 C99F null mutant mice, which are models that mimic the Phf6 C99F point mutation in human BFLS and lack PHF6 protein expression due to protein decay (Cheng et al., 2018). We also found that Phf6 C99F null mutant mice had significantly more Egr1-positive and cFos-positive AgRP neurons in the ARC under fed conditions (Figures S3B and S3C). To determine if the PHF6-mediated regulation of IEG expression also existed in other brain regions, we measured the number of Egr1-positive neurons in the SON in the Phf6 C99F null mutant mice. We found that PHF6 depletion also increased the number of Egr1-positive neurons in the SON, similar to that in the ARC (Figures S3D and S3E), indicating a general function of PHF6 in regulating IEG expression.

These results provide us with a scheme that the constitutive increase in IEGs impairs their further robust induction in response to external stimuli. We reasoned that in WT mice, PHF6 is a transcriptional repressor or part of a repressive complex, and the IEGs that are ordinarily induced by hunger are suppressed by PHF6 in the basal satiety state. In the absence of PHF6, the Phf6^{cKO} AgRP neurons constitutively express high levels of IEGs, which cannot be further activated in the hunger state.

PHF6 Binds to the Promoters of a Subset of IEGs in the Hypothalamus

To gain more insight into how PHF6 regulates the expression of downstream genes, particularly IEGs, we performed ChIP-seq using anti-PHF6 antibodies on the enriched ARC tissues

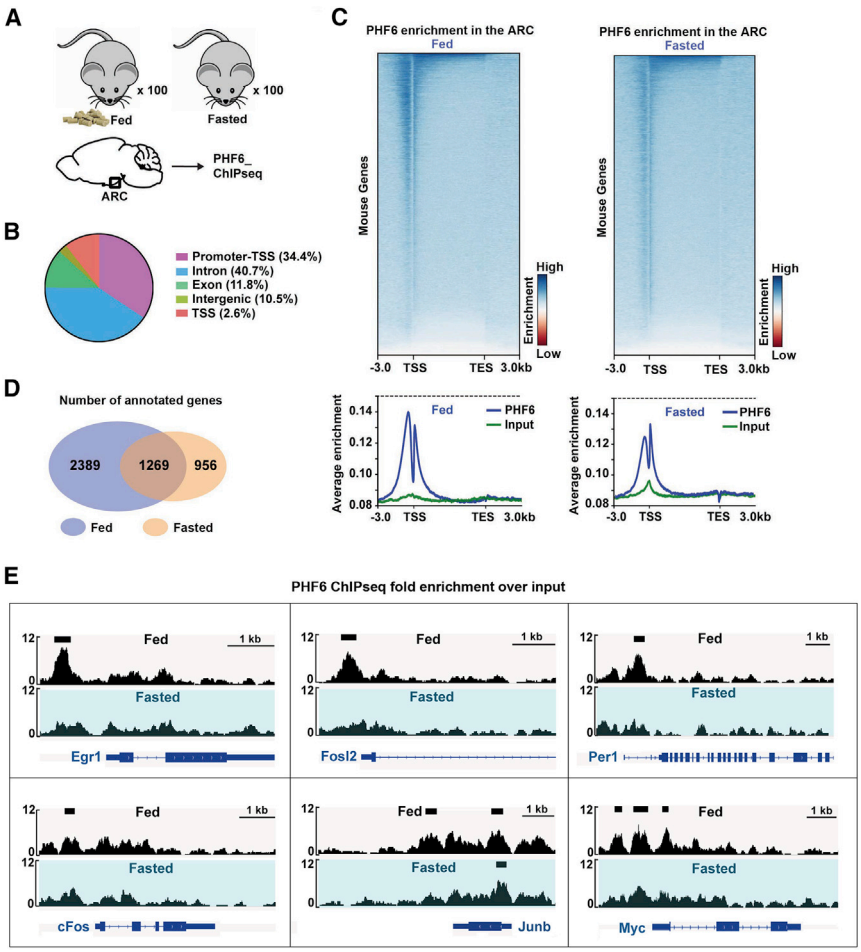

Figure 4. PHF6 Binds to the Promoters of a Subset of IEGs

(A) Illustration of ChIP-seq with an anti-PHF6 antibody on the enriched ARC tissue from 100 fed and 100 fasting WT mice.

(B) Genome-wide distribution of PHF6 occupancy in the ARC of the hypothalamus.

(C) Heatmaps for genome-wide PHF6 enrichment in the ARC from normalized PHF6 ChIP-seq reads in fed and fasting conditions are shown. PHF6 occupancy from 3 kb upstream of the transcription start site (TSS) and 3 kb downstream of the transcription end site (TES) are shown. Bottom panels show the average enrichment of PHF6 over input in fed and fasting conditions.

(D) Pairwise comparison of PHF6 ChIP-seq under fed and fasting conditions revealed 1269 overlapping, 2389 fed-condition-only, and 956 fasting-condition-only annotated genes.

(E) Examples of PHF6 ChIP-seq fold enrichment over input in the gene loci of Egr1, cFos, Fosl2, Junb, Per1, and Myc in fed and fasting conditions. PHF6 occupancy in the promoter regions of some IEGs was markedly decreased under fasting conditions compared to fed conditions. The black bar indicates the significant PHF6 binding peaks that were called.

See also Figure S4 and Table S4.

dissected from 100 fed and 100 fasted WT mice (Figure 4A). We characterized the genome-wide occupancy of PHF6 in the ARC of the hypothalamus. We found that a substantial number of PHF6-binding sites overlapped with the promoters and introns (Figure 4B). Under both fed and fasted conditions, the occupancy of PHF6 predominantly surrounded the transcription start sites (TSSs) near the promoter regions of most annotated genes (Figure 4C). Next, we performed integrative analyses between PHF6 ChIP-seq from WT mice and RNA-seq from $Phf6^{cKO}$ and $Phf6^{WT}$ mice. We found that the PHF6 directly regulates the expression of 73 $Phf6^{cKO}$-related differentially expressed genes in AgRP neurons because PHF6 directly bound to the promoter regions of these genes (Table S2).

To determine whether PHF6 has any DNA-sequence-specific binding properties in the hypothalamus, we performed Hypergeometric Optimization of Motif EnRichment (HOMER) motif enrichment analysis on the genomic sequences of PHF6-binding peaks. Although there were many DNA-binding motifs that passed the significance threshold, we found that most of the PHF6-chromatin-binding motifs showed a resemblance to the motifs bound by known transcription factors (Table S4). We found that PHF6-chromatin-binding sites in the hypothalamus displayed a broadly tuned rather than a sequence-specific property. It was similar to the findings in a previous study showing that PHF6 was unable to recognize specific DNA motifs in the blood B-ALL cells (Soto-Feliciano et al., 2017). These results suggest that PHF6 is a chromatin-binding protein that regulates transcription rather than a typical DNA-binding transcription factor, irrespective of the tissue expressing PHF6.

Hunger Triggers the Release of PHF6 from the Promoters of Certain IEGs

Pairwise comparison of PHF6 ChIP-seq analyses under both fed and fasted conditions revealed slightly distinct genomic-binding profiles of PHF6 in the hypothalamus (Figure 4C). The average enrichment of PHF6 near the TSSs of all the annotated genes under fasting conditions was moderately reduced compared to that under fed conditions (Figure 4C). We unveiled a combination of 1269 overlapping, 2389 fed-condition-only, and 956 fasted-condition-only binding sites from PHF6 ChIP-seq analyses in different nutritional states (Figure 4D; Table S4). For the 1269 overlapping PHF6-binding sites in fed and fasted conditions, we found that most of them displayed reduced PHF6 occupancy levels in the fasted condition compared to those in the fed condition (Figure S4A). These findings suggest that the PHF6-chromatin interaction in AgRP neurons is dynamically regulated in different nutritional states of the mice.

We next asked whether PHF6 bound to the promoters of particular IEGs and whether this binding was regulated by the hunger state. We analyzed the PHF6 ChIP-seq fold enrichment

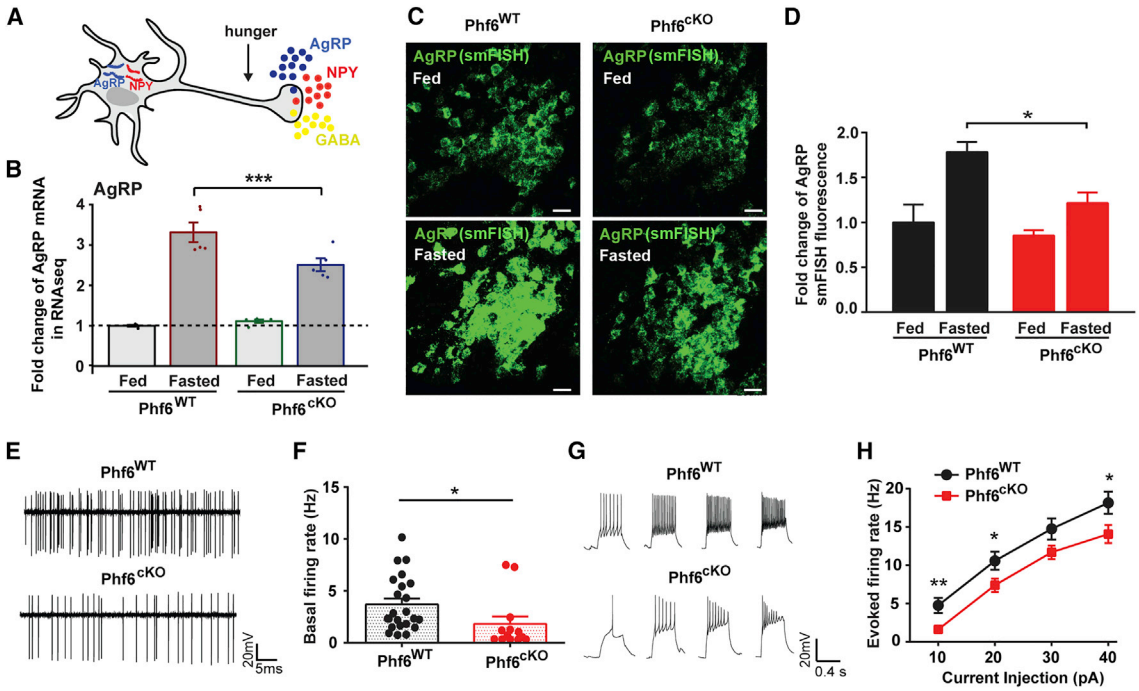

Figure 5. Decreased AgRP Induction and Reduced Neuronal Activity upon PHF6 Loss

(A) A model AgRP neuron that releases AgRP, NPY, and GABA in response to hunger.

(B) Fold change in normalized counts of RNA-seq reads of the AgRP gene under fed and fasting conditions in Phf6^{WT} and Phf6^{cKO} mice. Loss of Phf6 impaired the increase of AgRP mRNA level in fasting conditions ($p < 0.001$) (n = 5 for Phf6^{WT}, n = 5 for Phf6^{cKO}).

(C and D) Detection of AgRP mRNA by smFISH (RNAscope) (C) and the quantification of fold change in AgRP mRNA fluorescence signal (D) in fed and fasting conditions from Phf6^{WT} and Phf6^{cKO} mice. Scale bars are 25 μm (C). Loss of Phf6 significantly impaired the increase in AgRP mRNA in response to hunger ($p < 0.05$) (n = 3 for Phf6^{WT}-fed, n = 3 for Phf6^{cKO}-fed, n = 3 for Phf6^{WT}-fasted, n = 3 for Phf6^{cKO}-fasted).

(E and F) Representative traces (E) and the quantification (F) of spontaneous firing rate by loose-patch recording in tdTomato^{+} AgRP neurons from Phf6^{WT} and Phf6^{cKO} mice in hunger state.

(G and H) Representative traces (G) and the quantification (H) of evoked firing rate by whole-cell patch clamp recording with injecting depolarizing current in tdTomato^{+} AgRP neurons from Phf6^{WT} and Phf6^{cKO} mice.

Data are represented as mean ± SEM. See also Figure S5.

over input and found that PHF6 indeed bound to the promoter regions of a subset of activity-dependent IEGs including Egr1, Fosl2, Per1, cFos, Junb, and Myc (Figure 4E). The observation of PHF6 occupancy on the IEG promoters and the increase of IEG expression upon PHF6 loss strongly indicate that PHF6 functions as a repressor or part of a repressive complex to suppress the expression of these IEGs. Strikingly, we found that PHF6-chromatin binding was dynamically regulated by hunger state. Hunger triggered a significant reduction in PHF6 occupancy on the promoter regions of some IEGs, including Egr1, Fosl2, and Per1 (Figures 4E and S4B), while hunger triggered a slight reduction of PHF6 occupancy on the promoter regions of other IEGs, including cFos, Junb, and Myc (Figures 4E and S4B). These results suggest that the hunger state triggers the release of repressive PHF6 from the IEG promoters to facilitate their rapid and robust induction.

Decreased AgRP Induction and Reduced Neuronal Activity upon PHF6 Loss

Because the rapid induction of activity-dependent IEGs is followed by a second wave of expression of late-response genes that contribute to neuronal activity and the appropriate behavioral outcomes, we asked whether a loss of PHF6 in AgRP neurons would influence the expression of downstream genes. It is known that the activation of AgRP neurons elicits a rapid eating response mediated by the release of GABA and NPY, while a slower onset and more sustained eating response is mediated by the release of AgRP (Figure 5A; Atasoy et al., 2012; Krashes et al., 2013). Analysis of AgRP mRNA levels from the RNA-seq results showed that the magnitude of hunger-induced AgRP fold change in Phf6^{cKO} mice was decreased compared to that in Phf6^{WT} mice (Figure 5B). We performed single molecular fluorescence *in situ* hybridization (smFISH) with a mouse AgRP probe to further verify this observation. Compared to Phf6^{WT} mice, Phf6^{cKO} mice showed reduced fold change of AgRP mRNA level in the hunger state (Figures 5C and 5D). Notably, the basal mRNA and protein levels of endogenous AgRP were similar between Phf6^{WT} and Phf6^{cKO} mice in the satiety state (Figures 5B–5D and S5E). In contrast to IEG regulation, PHF6 might not directly regulate the AgRP gene transcription due to the lack of PHF6 chromatin-binding peaks around the AgRP gene in ChIP-seq data. We believe that the constitutive IEG activation and the

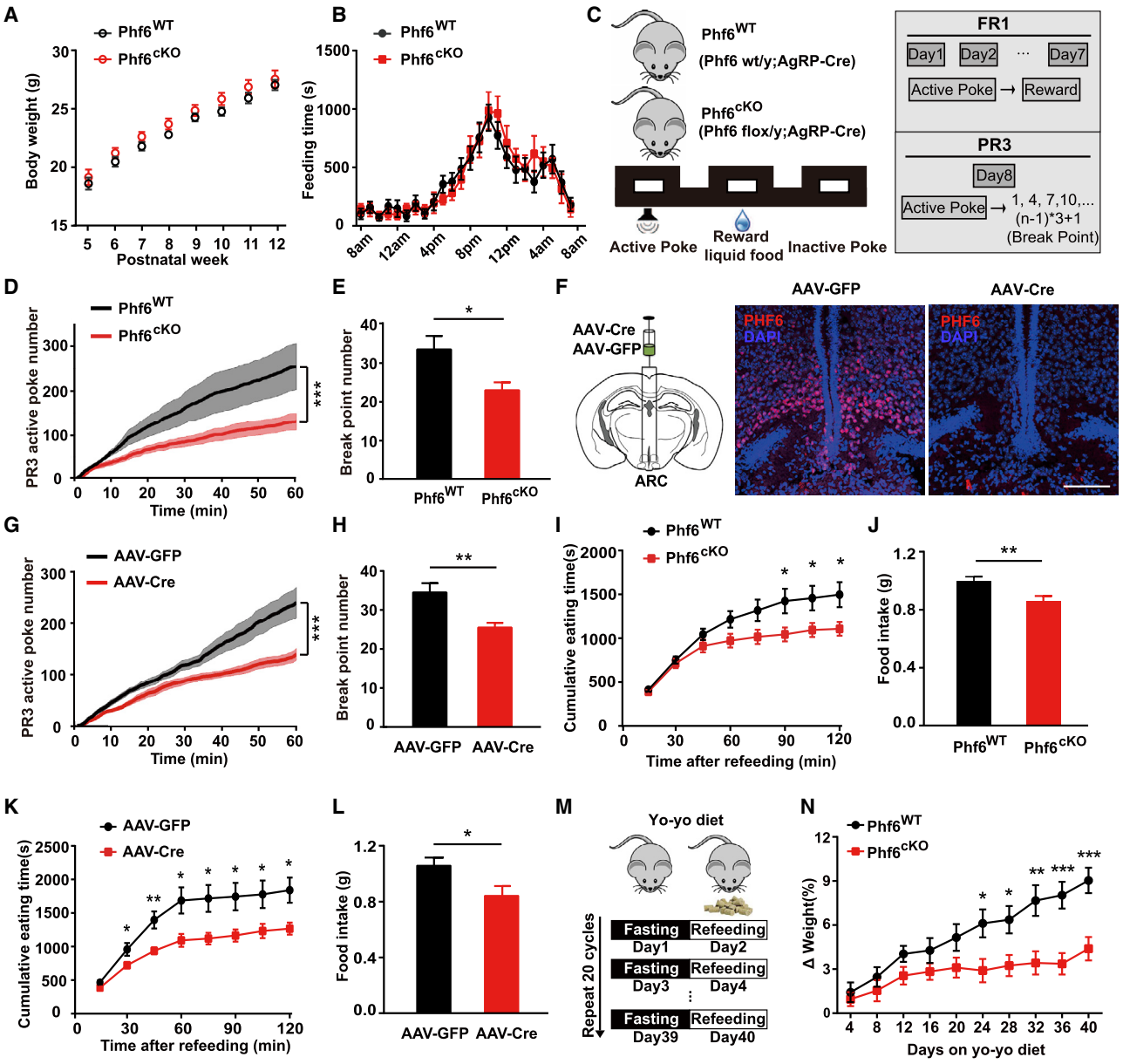

Figure 6. Loss of PHF6 in AgRP Neurons Attenuates Hunger-Driven Feeding Behavior

(A) Body weight of Phf6^{WT} mice (n = 12) and Phf6^{cKO} mice (n = 10) from postnatal weeks 5 to 12.

(B) Distribution of homeostatic eating time during the 24-h day-night cycle (n = 21 for Phf6^{WT}, n = 21 for Phf6^{cKO}).

(C) Illustration of hunger-driven motivation behavior for food seeking with the FR1 training schedule and the PR3 reinforcement schedule.

(D and E) cKO of Phf6 in AgRP neurons significantly decreased the cumulative active poke number (D; $p < 0.001$) and break point (E; $p < 0.05$) in the PR3 test in Phf6^{cKO} mice compared to those in Phf6^{WT} mice (n = 13 for Phf6^{WT}; n = 9 for Phf6^{cKO}).

(F) Depletion of Phf6 by injecting AAV-Cre virus into the ARC of 2-month-old Phf6$^{flox/y}$ male mice. Immunofluorescence of PHF6 showed the AAV-Cre virus-induced depletion of Phf6 in the ARC. The scale bar is 100 μm.

(G and H) Depletion of Phf6 by injection of AAV-Cre virus in the ARC of adult Phf6$^{flox/y}$ mice significantly decreased the cumulative active poke number (G; $p < 0.001$) and break point (H; $p < 0.01$) in the PR3 test (n = 6 for AAV-GFP; n = 6 for AAV-Cre).

(I) Cumulative eating time during the 2-h refeeding test after overnight fasting was decreased in Phf6^{cKO} mice (n = 15) compared to that in Phf6^{WT} mice (n = 20) during the time course from 90 to 120 min after the onset of refeeding ($p < 0.05$).

(J) Weight of food intake during the 2-h period of refeeding after overnight fasting was decreased in Phf6^{cKO} mice (n = 15) compared to that in Phf6^{WT} mice (n = 21) ($p < 0.01$).

(K and L) Depletion of Phf6 in adult mice by AAV-Cre viral infection decreased the cumulative feeding time during the time course from 30 to 120 min after the onset of refeeding (K; $p < 0.01$) and decreased the weight of food intake during the 2-h period of refeeding (L; $p < 0.05$) after overnight fasting compared to control AAV-GFP viral transfection (n = 7 for AAV-Cre; n = 8 for AAV-GFP).

(legend continued on next page)

unchanged AgRP expression in basal conditions in Phf6^{cKO} mice represent two different transcription regulatory patterns.

Furthermore, we measured the action potential firing rate in the Phf6^{WT} and Phf6^{cKO} AgRP neurons by performing lose-patch recording on tdTomato-positive AgRP neurons. We found that a loss of PHF6 significantly decreased the spontaneous action potential firing rate of AgRP neurons from mice in hunger (Figures 5E and 5F). To understand why Phf6^{cKO} neurons had a lower spontaneous firing rate, we analyzed the mRNA levels of the genes encoding ion channels from the RNA-seq results. We found that there were 19 Phf6^{cKO}-related differentially expressed genes encoding ion channel—including the potassium channel, chloride channel, calcium channel, GABA receptor, and glutamate receptor (Figure S4C)—suggesting that Phf6 loss may change the membrane excitability. In addition, we found that the action potential firing rate evoked by injecting the depolarizing current was lower in Phf6^{cKO} AgRP neurons compared to that in Phf6^{WT} AgRP neurons (Figures 5G and 5H). These results suggest that a loss of PHF6 reduces the excitability of AgRP neurons in the hunger state.

Moreover, we wanted to determine whether cKO of PHF6 influenced the proliferation and morphogenesis of AgRP neurons. We found that neither the total number of AgRP neurons within the ARC nor the gross pattern of axon projection of AgRP neurons was altered in Phf6^{cKO} mice compared to that in Phf6^{WT} mice (Figures S5A–S5D). Only a slightly different axon projection to the regions of the paraventricular nucleus of the thalamus (PVT) and the central nucleus of the amygdala (CeA) was observed in Phf6^{cKO} mice (Figure S5D). These findings suggest that cKO of PHF6 decreases the excitability of AgRP neurons without profound changes in the number and morphogenesis of AgRP neurons.

Loss of PHF6 in AgRP Neurons Attenuates Hunger-Driven Feeding Motivation

Given that Phf6-deficient AgRP neurons displayed a hunger-state shifting transcriptional profile, we predicted that a loss of PHF6 would promote homeostatic feeding behavior. Surprisingly, Phf6^{cKO} mice showed no significant difference in the body weight and day-night homeostatic eating under *ad libitum* feeding conditions compared to Phf6^{WT} mice (Figures 6A and 6B), suggesting that a loss of PHF6 in AgRP neurons does not alter homeostatic eating. Because Phf6^{cKO} AgRP neurons had higher absolute levels of IEGs but lower hunger-induced changes in IEG levels, we wanted to know whether the loss of PHF6 in AgRP neurons would influence motivational feeding in response to hunger stimulation.

We measured the hunger-driven feeding motivation in energy-deficient mice using the instrumental reinforcement paradigm. First, food-restricted Phf6^{cKO} mice or Phf6^{WT} mice were trained to associate a successful nose poke with the reward nutrient liquid using fixed ratio 1 (FR1) schedule. Second, after the FR1 training period, the same cohort of mice was tested on a progressive ratio 3 (PR3) reinforcement schedule (Figure 6C). We found that Phf6^{cKO} mice displayed a marked decrease in both the cumulative active poke number and the break point number during the PR3 test (Figures 6D and 6E). In addition to the above experiments using AgRP-Cre mice as Phf6^{WT} controls, the same result was obtained when we used another cohort of controls, Phf6$^{flox/y}$ mice (Figures S6A and S6B). To exclude the developmental defects caused by genetic knockout of Phf6, we used an alternative strategy to ablate Phf6 in adult mice by injecting of AAV-Cre virus into the ARC of the hypothalamus in young adult Phf6$^{flox/y}$ mice. AAV-Cre-induced depletion of Phf6 in the ARC was confirmed by immunohistochemistry (Figure 6F). We found that AAV-Cre-induced depletion of Phf6 in adult mice also decreased the cumulative active poke number and the break point number in the PR3 test (Figures 6G and 6H), recapitulating the behavioral phenotype in Phf6^{cKO} mice. The efficacy of AAV-Cre virus-mediated Phf6 depletion was verified by post hoc PHF6 immunostaining in each mouse. We found that the efficacy of Phf6 depletion by AAV-Cre had a negative correlation with the break point number in the PR3 test (Figure S6C). These results suggest that a loss of PHF6 in AgRP neurons attenuates hunger-driven feeding motivation in energy-deficient mice.

In addition, we measured hunger-driven motivational feeding using the overnight fasting and refeeding paradigm in Phf6^{WT} and Phf6^{cKO} mice. cKO of Phf6 in AgRP neurons decreased both cumulative eating time and the amount of food intake during the 2-h refeeding test after overnight fasting (Figures 6I and 6J). The same phenotypes of reduced hunger-driven refeeding were observed when we used AgRP-Cre mice (Figures 6I and 6J) and Phf6$^{flox/y}$ mice (Figures S6D and S6E) as two independent cohorts of controls. AAV-Cre-induced depletion of Phf6 in adult mice also reduced hunger-driven refeeding after overnight fasting (Figures 6K and 6L). These results demonstrate that a loss of PHF6 in AgRP neurons attenuates hunger-driven motivational feeding.

We performed further experiments to confirm the behavioral phenotypes observed in Phf6^{cKO} mice. First, we used the Phf6 C99F null mutant mice to measure the food intake during the 2-h refeeding after overnight fasting. Similar to Phf6^{cKO} mice, Phf6 C99F null mutant mice showed a reduced amount of food intake in the 2-h refeeding test (Figure S6F). Second, we performed two rescue experiments, in which exogenous PHF6 was overexpressed in AgRP neurons that lacked endogenous PHF6 expression by viral infection. In the 2-h refeeding test, expression of exogenous PHF6 in the PHF6-deficient mice reversed the cumulative eating time and the amount of food intake to the levels of the control mice (Figures S6G and S6H). In the hunger-driven feeding motivation test, expression of exogenous PHF6 in the PHF6-deficient mice also reversed the cumulative active poke number and the break point number during the PR3 test to the levels of the control mice (Figures S6I and S6J). Taken together, these results demonstrate that PHF6 in AgRP neurons regulates hunger-driven motivational feeding behavior.

(M) Illustration of yo-yo diet paradigm under repetitive fasting-refeeding conditions.
(N) Compared to Phf6^{WT} mice, Phf6^{cKO} mice displayed significantly reduced body weight gain on the yo-yo diet under repetitive fasting-refeeding conditions (n = 12 for Phf6^{WT}, n = 13 for Phf6^{cKO}) ($p < 0.001$).
Data are represented as mean ± SEM. See also Figure S6.

Loss of PHF6 in AgRP Neurons Makes the Mice Resistant to Body Weight Gain on a Yo-yo Diet

Furthermore, we wanted to determine if reduced hunger-driven feeding motivation in Phf6^{cKO} mice would influence body weight gain on a yo-yo diet under the repetitive fasting-refeeding conditions. A yo-yo diet paradigm mimics people who lose and regain weight repeatedly. Phf6^{cKO} and Phf6^{WT} littermates were subjected to intermittent (alternate day) fasting every other day and were provided *ad libitum* access to chow food the next day for 20 cycles in 40 days (Figure 6M). In contrast to the previous finding that Phf6^{cKO} mice showed unchanged body weight under normal *ad libitum* feeding conditions, Phf6^{cKO} mice displayed significantly reduced body weight gain while on the yo-yo diet, compared to Phf6^{WT}mice (Figure 6N). Loss of PHF6 in AgRP neurons makes the mice resistant to body weight gain, and it protects the mice against overeating under repetitive fasting-refeeding conditions. On the other hand, we found that Phf6^{cKO} mice showed no difference in high-fat-diet-induced body weight gain compared to Phf6^{WT} mice (Figure S6K). Taken together, our data demonstrate that a loss of PHF6 in AgRP neurons not only decreases hunger-driven feeding motivation, but also makes Phf6^{cKO} mice resistant to body weight gain under repetitive fasting-refeeding conditions (yo-yo diet).

DISCUSSION

In this study, we identified an AgRP neuron-enriched transcriptional repressor, PHF6, which regulates the adaptive response in hunger-driven feeding behavior (see model in Figure S6L). Through integrated RNA-seq and ChIP-seq analyses, we demonstrated that PHF6 bound to the promoters of a subset of IEGs, and the PHF6-chromatin binding was dynamically regulated by different nutritional states. Hunger triggered the decrease in PHF6 occupancy on the promoters of the IEGs and allowed for IEG rapid induction. Despite the unchanged body weight and homeostatic eating under normal *ad libitum* feeding conditions, Phf6^{cKO} mice displayed a significant reduction in hunger-driven motivational eating, and Phf6^{cKO} mice were resistant to body weight gain while on the yo-yo diet under repetitive fasting-refeeding conditions.

However, our findings elicit the question as to why the constitutive IEG activation in Phf6^{cKO} mice results in unchanged homeostatic eating under normal *ad libitum* feeding conditions but reduced hunger-driven eating under repetitive fasting-refeeding conditions. This apparent discrepancy may be explained by the following three reasons. (1) Although the IEGs are constitutively activated in PHF6-deficient AgRP neurons and PHF6 loss makes the AgRP neurons look transcriptionally more similar to AgRP neurons in the hunger state, there were still approximately 13% of the Phf6^{cKO}-related differentially expressed genes that showed opposite trends between changes in Phf6^{cKO}-fed versus Phf6^{WT}-fed and changes in Phf6^{WT}-fasted versus Phf6^{WT}-fed. Thus, the expected behavioral outcome might be compromised by these differently regulated genes. (2) Constitutive IEG activation in Phf6^{cKO} mice should be very different from transient IEG activation in a physiological behavioral state. Similar to the homeostatic plasticity theory that "sustained neural activity" triggers a "homeostatic decrease in synaptic excitability and strength," we speculate that "sustained IEG transcriptional activation" may also trigger "homeostatic adaptation in neuronal response to external stimuli." As a result, the constitutive IEG transcriptional activation in Phf6^{cKO} mice may desensitize the responsiveness of AgRP neurons toward hunger stimulation, leading to a very different behavioral outcome as observed in the transient IEG activation in response to a physiological stimulation. (3) It is the change in IEG levels, but not the absolute levels, which determines the behavioral outcome. Very few studies have reported the consequence of constitutive IEG activation in a particular neuronal subtype. Our study suggests that, at least in the AgRP neurons, the changes in the IEG levels, but not the absolute levels, are involved in regulating hunger-driven feeding motivation and resisting body weight gain under repetitive fasting-refeeding conditions.

Approximately 75% of the BFLS patients develop obesity emerging in late childhood (Jahani-Asl et al., 2016). However, we observed the phenotype of unchanged homeostatic eating and reduced hunger-driven motivational eating in the Phf6^{cKO} mice. We suspected that this discrepancy might be due to the difference between the germline mutations of Phf6 in BFLS patients and the cell-type-specific cKO of Phf6 in the mice. Patient obesity might be caused by an abnormal hormonal status and subsequent changes in metabolism because PHF6 is also highly expressed in the pituitary gland (Voss et al., 2007). Here, our data suggest that the function of PHF6 in the ARC of the hypothalamus is not responsible for the obesity symptoms observed in the BFLS patients.

In future studies, it will be interesting to identify how PHF6 functions as a transcriptional repressor or as part of a repressive complex to regulate hunger-dependent gene expression. It will also be interesting to know how different nutritional status regulates the endogenous level of PHF6 and how hunger signal triggers the release of PHF6 from the chromatin to facilitate the hunger-driven gene expression. Understanding these questions will shed light on the delicate interplay among the transcriptional regulation, the neuronal function, and adaptive behavioral responses in a physiological context.

STAR★METHODS

Detailed methods are provided in the online version of this paper and include the following:

- KEY RESOURCES TABLE
- LEAD CONTACT AND MATERIALS AVAILABILITY
- EXPERIMENTAL MODEL AND SUBJECT DETAILS
  - Mice
- METHOD DETAILS
  - Histology and immunostaining
  - Single molecular FISH (RNAscope)
  - Stereotaxic Surgeries
  - Homeostatic feeding
  - Hunger-driven motivational test
  - Overnight fasting/refeeding test
  - PHF6 rescue experiments
  - Yo-yo diet and high fat diet treatment
  - Dissociation and FACS sorting of AgRP neurons

SUPPLEMENTAL INFORMATION

Supplemental Information can be found online at https://doi.org/10.1016/j.celrep.2020.02.085.

ACKNOWLEDGMENTS

We thank Dr. Yu Fu in Singapore A*STAR for critical discussions and editing of the manuscript. We thank Dr. Jian-Fei Lu in SHSMU for drawing the model. This work was supported by grants from the Natural Science Foundation of China (81771215, 31771154, 31970933, 61721092, and 61890954), the Science and Technology Commission of Shanghai Municipality (18JC1420302), the program for Professor of Special Appointment (Eastern Scholar for J.H. and Q.L.) at Shanghai Institutions for Higher Learning (1710000221 and QD2018017), and the Shanghai Pujiang Program (17PJ1405300 and 17PJ1405400). This work was also supported by NHMRC Project grants (1029481 and 1084248) and NHMRC Research Fellowships (1003435 [T.T.], 1155224 [J.G.], and 575512 and 1081421 [A.K.V.]) and NIH grant NS088378 (A.B.). We also thank the innovative research team of high-level local universities in Shanghai for support.

AUTHOR CONTRIBUTIONS

J.H. designed and supervised the project; Q.L. performed bioinformatics analyses; L.G. performed the immunohistochemistry and molecular experiments; J.S. performed the behavioral experiments; S.Y. and X.Z. performed FACS sorting experiments; L.G., Y.S., and X.W. performed animal breeding and genotyping; W.C., J.Y., and A.L. performed fMOST experiments; M.A.C., M.P.D., T.T., A.K.V., and J.G. generated the Phf6 floxed mice; C.C. and A.B. generated the Phf6-C99F mutant mice; J.H. wrote the article; Q.L., A.K.V., and J.G. helped to edit the manuscript.

DECLARATION OF INTERESTS

The authors declare no competing interests.

Received: August 26, 2019
Revised: December 22, 2019
Accepted: February 24, 2020
Published: March 17, 2020

REFERENCES

Aponte, Y., Atasoy, D., and Sternson, S.M. (2011). AGRP neurons are sufficient to orchestrate feeding behavior rapidly and without training. Nat. Neurosci. *14*, 351–355.

Atasoy, D., Betley, J.N., Su, H.H., and Sternson, S.M. (2012). Deconstruction of a neural circuit for hunger. Nature *488*, 172–177.

Cheng, C., Deng, P.Y., Ikeuchi, Y., Yuede, C., Li, D., Rensing, N., Huang, J., Baldridge, D., Maloney, S.E., Dougherty, J.D., et al. (2018). Characterization of a Mouse Model of Borjeson-Forssman-Lehmann Syndrome. Cell Rep *25*, 1404–1414.e1406.

Gropp, E., Shanabrough, M., Borok, E., Xu, A.W., Janoschek, R., Buch, T., Plum, L., Balthasar, N., Hampel, B., Waisman, A., et al. (2005). Agouti-related peptide-expressing neurons are mandatory for feeding. Nat. Neurosci. *8*, 1289–1291.

Henry, F.E., Sugino, K., Tozer, A., Branco, T., and Sternson, S.M. (2015). Cell type-specific transcriptomics of hypothalamic energy-sensing neuron responses to weight-loss. eLife *4*.

Hrvatin, S., Hochbaum, D.R., Nagy, M.A., Cicconet, M., Robertson, K., Cheadle, L., Zilionis, R., Ratner, A., Borges-Monroy, R., Klein, A.M., et al. (2018). Single-cell analysis of experience-dependent transcriptomic states in the mouse visual cortex. Nat. Neurosci. *21*, 120–129.

Jahani-Asl, A., Cheng, C., Zhang, C., and Bonni, A. (2016). Pathogenesis of Börjeson-Forssman-Lehmann syndrome: Insights from PHF6 function. Neurobiol. Dis. *96*, 227–235.

Kim, T.K., Hemberg, M., Gray, J.M., Costa, A.M., Bear, D.M., Wu, J., Harmin, D.A., Laptewicz, M., Barbara-Haley, K., Kuersten, S., et al. (2010). Widespread transcription at neuronal activity-regulated enhancers. Nature *465*, 182–187.

Krashes, M.J., Koda, S., Ye, C., Rogan, S.C., Adams, A.C., Cusher, D.S., Maratos-Flier, E., Roth, B.L., and Lowell, B.B. (2011). Rapid, reversible activation of AgRP neurons drives feeding behavior in mice. J. Clin. Invest. *121*, 1424–1428.

Krashes, M.J., Shah, B.P., Koda, S., and Lowell, B.B. (2013). Rapid versus delayed stimulation of feeding by the endogenously released AgRP neuron mediators GABA, NPY, and AgRP. Cell Metab. *18*, 588–595.

Luquet, S., Perez, F.A., Hnasko, T.S., and Palmiter, R.D. (2005). NPY/AgRP neurons are essential for feeding in adult mice but can be ablated in neonates. Science *310*, 683–685.

Madabhushi, R., and Kim, T.K. (2018). Emerging themes in neuronal activity-dependent gene expression. Mol. Cell. Neurosci. *87*, 27–34.

Madabhushi, R., Gao, F., Pfenning, A.R., Pan, L., Yamakawa, S., Seo, J., Rueda, R., Phan, T.X., Yamakawa, H., Pao, P.C., et al. (2015). Activity-Induced DNA Breaks Govern the Expression of Neuronal Early-Response Genes. Cell *161*, 1592–1605.

McRae, H.M., Garnham, A.L., Hu, Y., Witkowski, M.T., Corbett, M.A., Dixon, M.P., May, R.E., Sheikh, B.N., Chiang, W., Kueh, A.J., et al. (2019). PHF6 regulates hematopoietic stem and progenitor cells and its loss synergizes with expression of TLX3 to cause leukemia. Blood *133*, 1729–1741.

Soto-Feliciano, Y.M., Bartlebaugh, J.M.E., Liu, Y., Sánchez-Rivera, F.J., Bhutkar, A., Weintraub, A.S., Buenrostro, J.D., Cheng, C.S., Regev, A., Jacks, T.E., et al. (2017). PHF6 regulates phenotypic plasticity through chromatin organization within lineage-specific genes. Genes Dev. *31*, 973–989.

Sternson, S.M., and Eiselt, A.K. (2017). Three Pillars for the Neural Control of Appetite. Annu. Rev. Physiol. *79*, 401–423.

van den Top, M., Lee, K., Whyment, A.D., Blanks, A.M., and Spanswick, D. (2004). Orexigen-sensitive NPY/AgRP pacemaker neurons in the hypothalamic arcuate nucleus. Nat. Neurosci. *7*, 493–494.

Voss, A.K., Gamble, R., Collin, C., Shoubridge, C., Corbett, M., Gécz, J., and Thomas, T. (2007). Protein and gene expression analysis of Phf6, the gene mutated in the Börjeson-Forssman-Lehmann Syndrome of intellectual disability and obesity. Gene Expr. Patterns *7*, 858–871.

Wu, Y.E., Pan, L., Zuo, Y., Li, X., and Hong, W. (2017). Detecting Activated Cell Populations Using Single-Cell RNA-Seq. Neuron *96*, 313–329.e316.

Yap, E.L., and Greenberg, M.E. (2018). Activity-Regulated Transcription: Bridging the Gap between Neural Activity and Behavior. Neuron *100*, 330–348.

Zhang, C., Mejia, L.A., Huang, J., Valnegri, P., Bennett, E.J., Anckar, J., Jahani-Asl, A., Gallardo, G., Ikeuchi, Y., Yamada, T., et al. (2013). The X-linked intellectual disability protein PHF6 associates with the PAF1 complex and regulates neuronal migration in the mammalian brain. Neuron *78*, 986–993.

STAR★METHODS

KEY RESOURCES TABLE

REAGENT or RESOURCE	SOURCE	IDENTIFIER
Antibodies		
Rabbit anti PHF6 antibody	NOVUS	Cat# NB100-68262; RRID:AB_2165374
Rabbit anti PHF6 antibody	Sigma-Aldrich	Cat# HPA001023 RRID:AB_1079606
Rabbit anti c-Fos (9F6) antibody	Cell Signaling Technology	Cat# 2250; RRID:AB_2247211
Rabbit anti EGR1 (15F7) antibody	Cell Signaling Technology	Cat# 4153; RRID:AB_2097038
Mouse anti ACTH/CLIP (POMC)	Santa Cruz Biotechnology	Cat# SC-373878; RRID:AB_10917583
Goat anti AgRP antibody	Santa Cruz Biotechnology	Cat# SC-18634; RRID:AB_2258141
Goat anti-Rabbit IgG (H+L), Alexa Fluor 555	Thermo Fisher Scientific	Cat# A21428; RRID:AB_2535849
Goat anti-Mouse IgG (H+L), Alexa Fluor 488	Thermo Fisher Scientific	Cat# A11001; RRID:AB_2534069
Goat anti-Rabbit IgG (H+L), CoraLite 488	Proteintech	Cat# SA00013-2; RRID:AB_2797132
Donkey anti-Goat IgG (H+L), Alexa Fluor 647	Thermo Fisher Scientific	Cat# A-21447; RRID:AB_2535864
Bacterial and Virus Strains		
AAV2/9-CMV_bGI-Cre-eGFP	Shanghai Taitool Bioscience	Cat# S0231-9
AAV2/9-CMV_bGI-eGFP	Shanghai Taitool Bioscience	Cat# S0263-9
AAV2/9-EF1a-DIO-eGFP	Shanghai Taitool Bioscience	Cat# S0270-9
AAV2/9-EF1a-DIO-eGFP-2A-PHF6	Shanghai Taitool Bioscience	N/A
Chemicals, Peptides, and Recombinant Proteins		
RNAscope® H2O2 and Rrotease Reagents	Advanced Cell Diagnostics	Cat# 322381
RNAscope® Multiplex Fluorescent Detection Reagents v2	Advanced Cell Diagnostics	Cat# 323110
RNAscope® Wash Buffer Reagents	Advanced Cell Diagnostics	Cat# 310091
RNAscope® Multiplex TSA Buffer	Advanced Cell Diagnostics	Cat# 322809
Mm-AgRP-C3	Advanced Cell Diagnostics	Cat# 400711
TSA® Plus fluorescein System(FITC)	Perkin Elmer	Cat# NEL741E001KT
Probe Diluent (C1 Channel)	Advanced Cell Diagnostics	Cat# 300041
NEB/NEBNext® Library Quant Kit for Illumina®	NEB	Cat# E7630S
Papain Dissociation System kit	Worthington-Biochem	Cat# LK003150
TTX, NBQX, APV	Tocris	Cat# 1078, 1044, 0106
Actinomycin D	Tocris	Cat# 1229
SMART-seq v4 Ultra Low Input RNA kit	Clontech	Cat# 634888
AgencourtAMPure XP PCR purification kit	Beckman Coulter Item	Cat# A63880
Nextera® XT DNA Library Preparation Kit	Illumina	Cat# FC-131-1024
Deposited Data		
RNA-seq and ChIP-seq data	This paper	https://www.ncbi.nlm.nih.gov/geo/query/acc.cgi?acc=GSE139545
Deposited Data	This paper	https://doi.org/10.17632/fpndyzs4ht.1
Experimental Models: Organisms/Strains		
Mouse: C57BL/6J (B6/J)	Slac Laboratory Animal, Shanghai	N/A
Mouse: Phf6 flox/flox	Dr. Tim Thomas in The Walter and Eliza Hall Institute of Medical Research, Australia	N/A
Mouse: AgRP-IRES-Cre	Jackson Laboratory	Cat# JAX:012899
Mouse: Ai9 reporter	Jackson Laboratory	Cat# JAX:007909
Mouse: NPY-hrGFP	Jackson Laboratory	Cat# JAX:006417

(*Continued on next page*)

Continued

REAGENT or RESOURCE	SOURCE	IDENTIFIER
Mouse: Histone-GFP reporter	Dr. Miao He in Institutes of Brain Science of Fudan University, China	N/A
Mouse: Vglut2-IRES-Cre	Jackson Laboratory	Cat# JAX: 028863
Mouse: Vgat-IRES-Cre	Jackson Laboratory	Cat# JAX: 028862
Mouse: PHF6 C99F knock-in: B6.PHF6 (nt.296G > T)	Dr. Azad Bonni in Washington University School of Medicine, St. Louis, MO, USA.	N/A
Software and Algorithms		
GraphPad Prism 7	GraphPad	RRID: SCR_002798
Adobe Illustrator	Adobe	http://shop.adobe.com/store/adbehap/DisplayHomePage
Adobe Photoshop	Adobe	http://shop.adobe.com/store/adbehap/DisplayHomePage
ImageJ	NIH ImageJ	https://imagej.nih.gov/ij/index.html
LAS X	Leica	https://www.leica-microsystems.com/products/microscope-software/p/leica-las-x-ls/
MATLAB_R2016b	Mathworks	https://ww2.mathworks.cn/products/matlab.html
LabStatever 3.1 for Operant Behavior	AniLab software and Instruments Co., Ltd.	http://www.anilab.cnhome.asp
CinePlex Editor V3	Plexon	http://www.hkplexon.com
Allen Brain Atlas	Allen Institute for Brain Science	http://mouse.brain-map.org
KEGG Brite ko03000	KEGG	http://rest.kegg.jp/get/br:ko03000

LEAD CONTACT AND MATERIALS AVAILABILITY

Further information and requests for resources and reagents should be directed to and will be fulfilled by lead contact, Ju Huang (juhuang@shsmu.edu.cn). This study did not generate new unique reagents. We obtained Phf6 flox/flox mice from the lab of Dr. Tim Thomas under an MTA from WEHI Australia and Phf6 C99F mutant mice from the lab of Dr. Azad Bonni under an MTA from WUSTL USA.

EXPERIMENTAL MODEL AND SUBJECT DETAILS

Mice

All experimental protocols were approved by the Institutional Animal Care and Use Committee at Shanghai Jiaotong University School of Medicine (Protocol A-2016-044). Mice were housed on a 7am-7pm light/dark cycle with water and mouse chow *ad libitum*. The following mouse lines were used in this study (also see the mouse strains information in the Key Resources Table): wild-type C57BL/6J (B6/J) mice; Phf6^{cKO} mice (Phf6 flox/y; AgRP-Cre/+; Ai9/+); Phf6^{WT} mice (Phf6 wt/y; AgRP-Cre/+); PHF6-C99F mutant mice; NPY-hrGFP mice; Histone-GFP and Ai9 reporter mice; AgRP-IRES-Cre mice; Vglut2-IRES-Cre mice; and Vgat-IRES-Cre mice were used. To obtain the Phf6^{cKO} mice (Phf6 flox/y; AgRP-Cre/+; Ai9/+) and littermate control mice (Phf6 wt/y; AgRP-Cre/+; Ai9/+) in which tdTomato was expressed in the AgRP neurons, we crossed the female Phf6 flox/+ mice with the male AgRP-Cre/+; Ai9/Ai9 mice. To obtain the Phf6^{cKO} mice (Phf6 flox/y; AgRP-Cre/+) and littermate control mice (Phf6 wt/y; AgRP-Cre/+) mice without fluorescent protein labeling, we crossed the female Phf6 flox/+ mice with the male AgRP-Cre/Cre mice. To obtain the Phf6^{cKO} mice (Phf6 flox/y; AgRP-Cre/+) and littermate control Phf6 flox/y mice, we crossed the female Phf6 flox/flox mice with the male AgRP-Cre/+ mice.

METHOD DETAILS

Histology and immunostaining

Animals were perfused transcardially with 2% paraformaldehyde (PFA) followed by 2-hour post fixation for the experiments of endogenous PHF6, cFos, Egr1, POMC and AgRP immunostaining. 30-μm frozen sections were cut. Sections were blocked in 10% goat serum, 0.4% Triton x-100, and 0.3% BSA for 2 hours. We applied the PHF6 antibody (NOVUS, NB100-68262, 1:500), the Egr1 antibody (CST, mAb #4153S, 1:300), the POMC (ACTH) antibody (Santa Cruz, SC-373878; 1:500) and the AgRP antibody (Santa Cruz,

SC-18634; 1:500) overnight at 4°C, the cFos antibody (CST, mAb #2250, 1:300) overnight at 4°C and additional 5 hours at room temperature. Goat anti-rabbit 488 (1:500), goat anti-rabbit 555 (1:500), goat anti-mouse 488 (1:500) or donkey anti-goat 647 (1:500) and DAPI (1:10,000 of 5 mg/ml) were applied for 2 hours at room temperature. Confocal images were obtained with a Leica STED sp8 system.

Single molecular FISH (RNAscope)

Single molecular FISH (smFISH) was performed on fresh frozen sections from 4-week old $Phf6^{cKO}$ and $Phf6^{WT}$ mice using the RNAscope technique of Advanced Cell Diagnostics (Hayward, CA, United States). Briefly, animals were anesthetized and the brains were removed and immediately frozen on dry ice. The freshly frozen brain was transferred and buried into OTC and frozen on dry ice again. Frozen tissues were stored at −80°C for later use. 20-μm sections were cut and air-dried inside the cryostat (−20°C) for 20 minutes and then stored at −80°C. Sections were fixed in 4% PFA for 15 minutes at 4°C, dehydrated in ethanol series, H_2O_2 was added to each section for 10 minutes and the slides were washed in PBS. Protease III was added and incubated for 20 minutes at room temperature. Probes were mixed at a 1:50 ratio of Channel 2 or Channel 3 with Channel 1 probes. Sections were incubated with AgRP probe (Mm-AgRP-C3, #400711-C3) for 2.5 hours at 40°C in the HybEZ humidified incubator, then rinsed in ACD wash buffer, and sequentially incubated in reagents AMP1-FL, AMP2-FL and AMP3-FL for 30 minutes each followed by DAPI. Slides were applied for image acquisition at 20x and 40x using a Leica Sp8 confocal system.

Stereotaxic Surgeries

Standard stereotactic procedures were applied to mice under anesthesia (100 mg/kg sodium pentobarbital, i.p.). Body temperature was maintained stable using a temperature controller (RWD Instruments). For AAV-Cre injection, 400 nL of AAV-CMV_bGI-Cre-eGFP or control AAV-CMV_bGI-eGFP (3×10^{12} per ml) was bilaterally injected into the ARC of the hypothalamus (AP: −1.5 mm, ML: ± 0.25 mm, DV: −5.85 mm) at a rate of 40 nl/min using a Nanofil syringe injector (World Precision Instruments) and a Quintessential stereotaxic injector controller (Stoelting CO.). After surgery, mice were injected with Ketoprofen (5 mg/kg, i.p.) for postoperative analgesia. Three weeks after virus injection, mice were used in behavioral experiments. *Post hoc* PHF6 immunostaining was performed to confirm the effect of AAV-Cre-induced Phf6 depletion and the efficacy of AAV-Cre-induced Phf6 depletion was calculated.

Homeostatic feeding

Mice were housed in a custom-designed chamber individually with food and water *ad libitum*, and habituated for 3 days before behavioral experiments. For the 24-hour homeostatic feeding measurement, feeding was measured by monitoring the feeding counts and time with a set of infrared light beam-based system (Anilab Software & Instruments, China). When the head of mouse entered into the hole for eating food, the infrared beam was broken. The Anilab software recorded the frequency and duration of each bout of eating.

Hunger-driven motivational test

Hunger-driven motivational behavior was carried out in an operant conditioning chambers (Anilab Software & Instruments, China). Chambers had 2 nose-poke holes with a cue light inside and a central feeder. When the head of mouse poked into the hole, an infrared beam was broken, and the signal was recorded by Anilab software. One nose-poke hole was the correct one to obtain the delivery of liquid food reward (Abbott Ensure), while the other nose-poke hole was the false one without the link of liquid food reward. During the training and test sessions, mice were on a diet to get 70% (2.5 g) of usual dairy diet of standard grain-based chow. Food-restricted $Phf6^{cKO}$ or $Phf6^{WT}$mice were first trained to associate a successful nose poke with the reward of nutrient liquid using FR1 (Fixed Ratio 1) schedule, in which each liquid delivery required one nose poke, during 1-hour sessions for 7 consecutive days. After the FR1 training, the same cohort of mice were tested on a PR3 (progressive ratio 3) reinforcement schedule, in which each liquid delivery reinforce required 3 additional nose pokes than the previous reinforce during 1-hour sessions, i.e., 1, 4, 7, 10, 3(n-1)+1. Mice that failed to have a 4 to 1 correct to false nose poke ratio after 7 days of FR1 training were excluded from further PR3 testing. The number of breakpoint was determined as the highest number of pokes for getting liquid food during the 1-hour PR3 period.

Overnight fasting/refeeding test

For the overnight fasting/refeeding test, mice were fasted overnight (food deprivation was started from 5 pm the day before experiment but water was provided). Refeeding test after over-night fasting was conducted for 2 hours between 10 am to 12 pm with the supply of regular chow food. The weight of food intake was carefully measured after the 2-hour refeeding test. Feeding was measured by monitoring the feeding counts and time with a set of infrared light beam-based system (Anilab Software & Instruments, China). The Anilab software recorded the frequency and duration of each bout of eating.

PHF6 rescue experiments

In the PHF6 rescue experiment for the 2-hour refeeding test after overnight fasting, eight-week-old $Phf6^{flox/y}$ mice were equally divided into three groups and subjected to the following viral injection into the ARC. Control mice: AAV-CMV_bGI-EGFP viral injection; Cre-induced PHF6-depletion mice: AAV-CMV_bGI-Cre-EGFP and AAV-EF1a-DIO-EGFP viral injection; PHF6-rescue

mice: AAV-CMV_bGI-Cre-EGFP and AAV-EF1a-DIO-EGFP-2A-PHF6 viral injection. Three weeks after viral injection, mice were subjected to the 2-hour refeeding test after overnight fasting, as well as the hunger-driven motivational test using the FR1-PR3 schedule.

Yo-yo diet and high fat diet treatment

Eight week-old littermate $Phf6^{WT}$ and $Phf6^{cKO}$ mice were used in the yo-yo diet and high fat diet treatment. Regular chow diet was provided *ad libitum* until the age of 8 weeks old. In the experiment of yo-yo diet treatment, mice were subjected to intermittent (alternate-day) fasting every other day and provided access to chow food the second day after 24-hour fasting. In the period of 40 days, there were a total of 20 repetitive fasting/refeeding cycles. The mice were weighted every other day to measure the body weight. In the experiment of high fat diet treatment, 8 week-old mice were provided with high fat diet (Reserch Diet, D12492, rodent diet with 60 kcal% fat) *ad libitum* for a period of 8 weeks. Body weight of the mice was measured once a week during the 8-week of high fat diet.

Dissociation and FACS sorting of AgRP neurons

AgRP neurons were obtained by FACS-sorting tdTomato positive red fluorescent neurons from the hypothalamus of the P24-28 $Phf6^{cKO}$ mice (Phf6 flox/y;AgRP-Cre/+;Ai9/+) and littermate control $Phf6^{WT}$ mice (Phf6 wt/y;AgRP-Cre/+;Ai9/+). For mice in fasted condition, food deprivation was started from 5 pm the day before experiment, but water was provided. At 9 am the next day, mice were sacrificed and around 1 mm^3 tissue surround the ARC from each mouse was obtained with a 1mm-diatmeter micro punch in the ice-cold dissection solution (1x HBSS,10 mM HEPES, 23 mM D-glucose). Micro-dissected hypothalamic tissues from 5 mice of the same genotype were pooled together. Cell dissociation was conducted using Papain Dissociation System kit (Worthington-Biochem: #LK003150), and the cell dissociation procedure was conducted under the guidance of the kit. Briefly, micro-dissected tissues were incubated for 30 minutes at 34°C in the Papain/DNase solution with the addition of transcription inhibitor Actinomycin D (8 μM), neuronal activity inhibitor TTX (1 μM), glutamate receptor inhibitors NBQX (20 μM) and AVP (50 μM). We bubbled the solution with 95% O_2 / 5% CO_2 during the incubation. Then we performed gentle titration to get the dissociated hypothalamic neurons, and the dissociated neurons were washed twice in 1x HBSS with 10% FBS with the presence of transcription inhibitor and neuronal activity blockers. The dissociated neurons were finally collected into 600 μL Neuralbasal Medium with 10% FBS and submitted for FACS sorting using BACKMAN FLOW CYTOMETER SYSTEM. 1000 tdTomato positive red fluorescent AgRP neurons per sample were sorted and collected into 10 μL lysis buffer with the presence of RNase inhibitor (SMART-Seq v4 Ultra Low Input RNA kit, Clontech). FACS-sorted AgRP neurons were frozen in −80°C till the preparation for SMART-RNaseq.

RNaseq and data analysis

1000 tdTomato positive AgRP neurons per sample in 10 ul lysis buffer with the RNase inhibitor were submitted for cDNA synthesis by using SMART-seq v4 Ultra Low Input RNA kit (Clontech). First-strand cDNA synthesis was primed by the 3′ SMART-Seq CDS Primer II A and used the SMART-Seq v4 oligonucleotide for template switching at the 5′ end of the transcript. cDNAs were amplified by LD PCR. PCR II A amplified cDNA from the SMART sequences introduced by 3′ SMART-Seq CDS Primer II A and the SMART-Seq v4 oligonucleotide for 15 cycles. PCR-amplified cDNA was purified by immobilization on AMPure XP beads. The beads were then washed with 80% ethonal and cDNA is eluted with elution buffer. Amplified cDNAs were then validated using the Agilent 2100 Bioanalyzer and Agilent's High Sensitivity DNA kit. 5 ng full-length cDNA output for next-generation sequencing was processed with the Nextera XT DNA library preparation kit (Illumina). Libraries were sequenced on the Illumina HiSeqXten.

RNA-seq reads were trimmed by Trimmomatic (version 0.36) and then aligned to the mouse reference genome (GRCm38/mm10, downloaded from UCSC, http://genome.ucsc.edu/) using Hisat2 (version 2.1.0). Next, raw counts of genes were quantified using featureCounts from Subread package (version 1.6.2). Normalized counts were obtained by normalizing raw counts with size factors using the "median ratio method" in DESeq2 1.20.0 package. Subsequent differentiated expressed gene analysis was performed using DESeq2 with default settings. The statistical analyses were performed by the LRT and the Wald significance testes. Significantly changed genes were identified with q value (BH-adjusted p value) cutoff of 0.05. The original count data were transformed using regularized logarithm method to calculate z scores and plot heatmaps. Gene ontology (GO) analysis on differentiated expressed genes was carried out using GO over-representation test in clusterProfiler package (version 3.10.1). GSEA analysis was conducted using the GSEA software with default parameters. Statistical significance: cutoffs at FDR (p adj) < 0.05, log2 fold change ≤ -1 or ≥ 1, mean of normalized counts ≥ 100 the significantly downregulated or upregulated transcription factors and cofactors under fasted versus fed condition; cutoffs at FDR (p adj) < 0.05, fold change > 1.5 or < 0.67, mean of normalized counts ≥ 20 for RNaseq analyses of the differentially expressed genes in $Phf6^{cKO}$ versus $Phf6^{WT}$ mice.

PHF6 ChIPseq and data analysis

Chromatin immunoprecipitation (ChIP) with PHF6 antibody on enriched ARC tissue dissected within 3 hours from 100 fed and 100 fasted wild-type mice (6-7 weeks old), followed by high-throughput sequencing (ChIPseq). Within 3 hours in the morning (9am-12pm), 100 wild-type mice in each condition were sacrificed and around 1 mm^3 tissue of the ARC from each mouse was obtained with a 1 mm-diatmeter micro punch in the ice-cold dissection solution (1x HBSS,10 mM HEPES, 23 mM D-glucose). The micro-dissected ARC tissues from 100 mice were pooled together for further ChIP preparation. Samples were cross-linked for 10 minutes at room temperature with 1% formaldehyde solution, followed by 5 minutes of quenching with 125 mM glycine, then washed twice with

ice-cold PBS. Nuclei fraction were collected and then sonicated in ice-cold lysis buffer by the Bioruptor for 40 cycles of 30 s ON and 30 s OFF. Sonicated lysates were cleared once by centrifugation and incubated overnight at 4°C with magnetic beads bound with PHF6 antibody (Sigma Aldrich, HPA001023) to enrich for DNA fragments bound by PHF6. For the preparation of the magnetic beads bound with PHF6 antibody, 70 μL of Protein G Dynabeads (Life Technologies) was blocked with 0.5% (w/v) BSA in PBS first, and then the magnetic beads were bound with 5 μg PHF6 antibody. After overnight incubation with the cleared sonicated lysates, the PHF6 antibody-bound magnetic beads were washed with RIPA buffer and then 1 M NH_4HCO_3. DNA was eluted in elution buffer. Cross-links were reversed overnight. Protein was digested using Proteinase K, and DNA was purified with HiPure Gel Pure DNA Mini Kit. Purified ChIP DNA was used to prepare Illumina multiplexed sequencing libraries. Libraries were prepared following the NEB/NEBNext® Library Quant Kit for Illumina®(E7630S). Amplified libraries were size-selected using a 2% gel to capture fragments between 200 bp and 500 bp. Libraries were quantified by Agilent 2100 and then sequenced on the Illumina HiSeq2500.

ChIPseq reads were mapped to the mouse reference genome (GRCm38/mm10, downloaded from UCSC, http://genome.ucsc.edu/) using Bowtie 2 (version 2.2.9) with the following parameters:–local –X 2000. Significant peaks were called using MACS2 (version 2.1.1.20160309) with "-f BAMPE" option and default threshold of *q* value (BH-adjusted *p* value) cutoff at 0.05. The peaks around transcription start sites were plotted using deeptools (version 2.5.3). And the peaks were annotated using annotatePeaks.pl function from HOMER (version 4.9) with default parameters. The HOMER's findMotifsGenome.pl tool was used for Motif analysis (the input file was the peak file and the genome fasta file). The DNA sequence was extracted according to the peak file, and the sequence was compared with the Motif database to obtain the known Motifs and *de novo* motifs. The bedgrap file containing the signal ratio of ChIP to Input samples was acquired using MACS2 WITH "bdgcmp -m FE" option.

Electrophysiology

We used P30-35 gender-matched littermate mice for the measurement spontaneous and evoked firing rate. Mice were sacrificed in hunger state at 5 pm before their meal in the evening. Acute 300 μm-thick hypothalamic slices were prepared by vibratome (Leica; VT1200) in cold high-Mg^{2+} and low-Ca^{2+} slicing solution containing 83 mM NaCl, 2.4 mM KCl, 0.5 mM $CaCl_2$, 6.8 mM $MgCl_2$, 24 mM $NaHCO_3$, 1.61 mM NaH_2PO_4, and 24 mM D-glucose and 65 mM sucrose, and then allowed to recover for 1 hour at 37°C in artificial cerebrospinal fluid (ACSF) containing 126 mM NaCl, 2.5 mM KCl, 1.2 mM NaH_2PO_4, 26 mM $NaHCO_3$, 1.3 mM $MgCl_2$, 2.5 mM $CaCl_2$, and 10 mM D-glucose, saturated in 95% O_2 / 5% CO_2. For recording, slices were perfused with O_2-saturated ACSF at a rate of 2 ml/min and maintained at 30°C. Recording electrodes (3-4 MΩ) were filled with internal solution containing 125 mM K-gluconate, 15 mM KCl, 10 mM HEPES, 2 mM ATP-Mg, 0.3 mM GTP-Na_3, 10 mM Na_2-phosphocreatine, and 0.2 mM EGTA. Series resistance in whole-cell patch-clamp recording was < 30 MΩ, and remained stable during the time course of the experiments. Electrophysiological signals were acquired by Axon MultiClamp 700B amplifier, digitized at 10 kHz by a Digidata 1440A D-A converter, and Bessel filtered at 2 kHz.

Whole-brain axon projection mapping by fMOST

The methods of preparing brain samples include irrigation, fixation, staining, dehydration, embedding and polymerization were described previously. Briefly, the mice were intracardially perfused with 4% PFA and 2% sucrose in 0.01 M PBS, followed by post fixation in 4% PFA at 4°C for 24 h. The brains were then dehydrated in a graded ethanol series (50, 70, and 95% ethanol at 4°C for 1 hour each), and then immersed in a graded glycol methacrylate (GMA, Ted Pella, United States) series, including 0.2% Sudan Black B (SBB, 70, 85, and 100% GMA for 2 hour each and 100% GMA overnight at 4°C). The samples were impregnated in a prepolymerization GMA solution for 3 days at 4°C and embedded in a vacuum oven at 48°C for 24 hours. The resin-embedded brain samples were imaged using the brain position system (BPS), a three-dimensional dual-color fluorescence microscope that sectioned and scanned the sample layer by layer until the data acquisition was completed. We acquired coronal image via a water immersion objective (1.0 NA, 20X), and sectioned the sample to remove the imaged tissue at 2 μm. The voxel resolution of the RAW data is 0.32 × 0.32 × 2 μm^3. Data analysis mainly included two steps of registration and signal density calculation. We registered the BPS dataset to the Allen CCF v3 reference atlas by using the BrainMapi method. A linear and nonlinear registration method was used to map and warp the extracted feature regions, and the accurate linear and nonlinear parameters were obtained. We applied the linear mat and nonlinear displacement to the original dataset directly or the Allen annotation file inversely to acquire the final registration results. We applied the threshold segmentation approach to each coronal plane to segment fluorescence signals from background. The segmented images were used to calculate the signal density in each interest brain region.

QUANTIFICATION AND STATISTICAL ANALYSIS

The data were analyzed using unpaired Student's t test in Figures 1F, 1G, 1I, 3E, 3G, 5B, 5D, 5F, 6E, 6H, 6J, 6L, S3B, S3C, S3E, S5B, S6B, S6E, and S6F; Wald significance testes in Figures 2D, 2E, and 3B; One-way analysis of variance (ANOVA) with *Tukey*'s test in Figures 1H, S6H, and S6J; Two-way ANOVA with *Tukey*'s multiple comparisons test in Figures 5H, 6A, 6B, 6I, 6K, 6N, S6D, S6G, and S6K. *Kolmogorov-Smirnov* test was used to compare the cumulative numbers of active pokes in hunger-driven motivational behavior in Figures 6D, 6G, S6A, and S6I. Linear regression and *Pearson* correlation were calculated by MATLAB for data analyses in Figures S1A and S6C. Data is judged to be statistically significant when $p < 0.05$. Statistical significance for RNaseq analyses: cutoffs at FDR (*p* adj) < 0.05, log2 fold change ≤ -1 or ≥ 1, mean of normalized counts ≥ 100 in Figure 1B; cutoffs at FDR (*p* adj) < 0.05, fold

change > 1.5 or < 0.67, mean of normalized counts ≥ 20 in Figures 2D and 2E; cutoffs at FDR (*p* adj) < 0.05, fold change > 1.5, mean of normalized counts ≥ 20 in Figure 2F. In all figures, asterisks denote statistical significance as *p < 0.05, **p < 0.01, ***p < 0.001. All statistical analysis was performed using GraphPad PRISM 7 software or MATLAB_R2016b or R (version 3.5.1). All statistical data are presented as mean ± SEM.

DATA AND CODE AVAILABILITY

The accession number for the RNA-seq and ChIP-seq data reported in this paper is Gene Expression Omnibus (GEO): GSE139545 (https://www.ncbi.nlm.nih.gov/geo/query/acc.cgi?acc=GSE139545).

All the original data (uncropped, unmodified images) for figures were deposited in Mendeley Data (https://doi.org/10.17632/fpndyzs4ht.1).